analytical chemistry

pubs.acs.org/ac Article

Programmable DNA Circuits for Flexible and Robust Exciton–Plasmon Interaction-Based Photoelectrochemical Biosensing

Hongbo Li,* Ye Cao, Tianyu Wu, Yansong Zhang, Zhaoting Zheng, Jingchun Lv, Airong Mao, Yuye Zhang, Qin Tang, and Jing Li*

Cite This: *Anal. Chem.* 2021, 93, 11043–11051 Read Online

ACCESS | Metrics & More | Article Recommendations | Supporting Information

ABSTRACT: DNA circuits as one of the dynamic nanostructures can be rationally designed and show amazing geometrical complexity and nanoscale accuracy, which are becoming increasingly attractive for DNA entropy-driven amplifier design. Herein, a novel and elegant exciton–plasmon interaction (EPI)-based photoelectrochemical (PEC) biosensor was developed with the assistance of a programmable entropy-driven DNA amplifier and superparamagnetic nanostructures. Low-abundance miRNA-let-7a as a model can efficiently initiate the operation of the entropy-driven DNA amplifier, and the released output DNAs can open the partially hybridized double-stranded DNA anchored on Fe_3O_4@SiO_2 particles. The liberated Au nanoparticles (NPs)-cDNA can completely hybridize with CdSe/ZnS quantum dots (QDs)-cDNA-1 and result in proportionally decreased photocurrent of CdSe/ZnS QDs-cDNA-1. This unique entropy-driven amplification strategy is beneficial for reducing the reversibility of each step reaction, enables the base sequence invariant and the reaction efficiency improvement, and exhibits high thermal stability and specificity as well as flexible design. These features grant the PEC biosensor with ultrasensitivity and high selectivity. Also, instead of solid–liquid interface assembly for conventional EPI-based PEC biosensors, herein, DNA hybridization in the solution phase enables the improved hybridization efficiency and sensitivity. In addition, superparamagnetic Fe_3O_4@SiO_2 particles further ensure the enhancement of the selectivity and reliability of the as-designed PEC biosensor. Particularly, this single-step electrode modification procedure evidently improves the electrode fabrication efficiency, reproducibility, and stability.

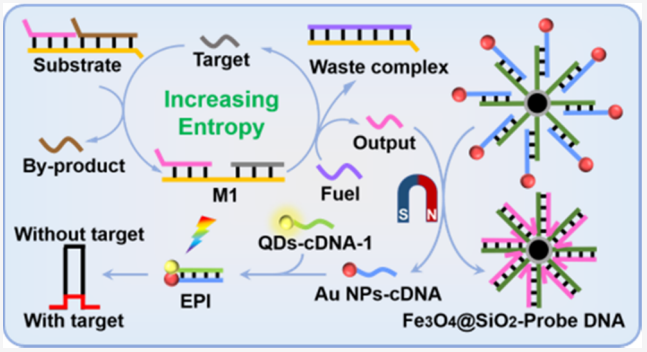

DNA molecules are significantly important in the life system, as they can carry genetic information.[1] Besides, they can be used for high-capacity information storage in nanotechnology.[2,3] Interestingly, DNA molecules can also be assembled to various predictable, biocompatible, and functional nanostructures.[4,5] At the beginning of the 1980s, Seeman reported the pioneering work of bottom-up predesigned and self-assembled nanomaterials according to the Watson–Crick base pairing rule.[6] This innovative idea benefits from the programmed and unique hybridization of complementary DNA strands.[7−9] DNA nanotechnology has experienced the initial self-fabrication of static structures,[10] and it is now becoming increasingly attractive for dynamic ones in engineering systems.[8,11] Recently, DNA circuits as one of the dynamic nanoscale structures have been reasonably engineered based on DNA strand displacement reactions.[12] This working principle grants the kinetic control of reaction routes. DNA circuits show amazing geometrical complexity and nanoscale accuracy,[13−15] and they are becoming increasingly attractive for DNA entropy-driven amplifiers applied in biosensors for the detection of microRNAs.[16−19] An entropy-driven amplifier is based on dynamic DNA assembly for a multichain composite structure,[20] which is different from the DNA hairpin structure for catalytic hairpin assembly (CHA) or hybridization chain reaction (HCR) biosignal amplification strategies.[21] Also, this unique strategy makes the signal amplification process irreversible.[22] Instead of forming new base pairs with the free energy release (CHA and HCR),[23] the unparalleled increasing entropy principle enables the base sequence invariant and the reaction efficiency improves.[24] Additionally, compared to CHA and HCR biosignal amplification techniques, entropy-driven DNA amplifiers exhibit high thermal stability and specificity for various measurements as well as flexible design.[25]

A vigorous photoelectrochemical (PEC) sensing technique evolved from electrochemical analysis has aroused increasingly research interest because the separation of light irradiation and

Received: June 13, 2021
Accepted: July 19, 2021
Published: July 28, 2021

Scheme 1. Schematic Illustration of the PEC Biosensor for miRNA-let-7a

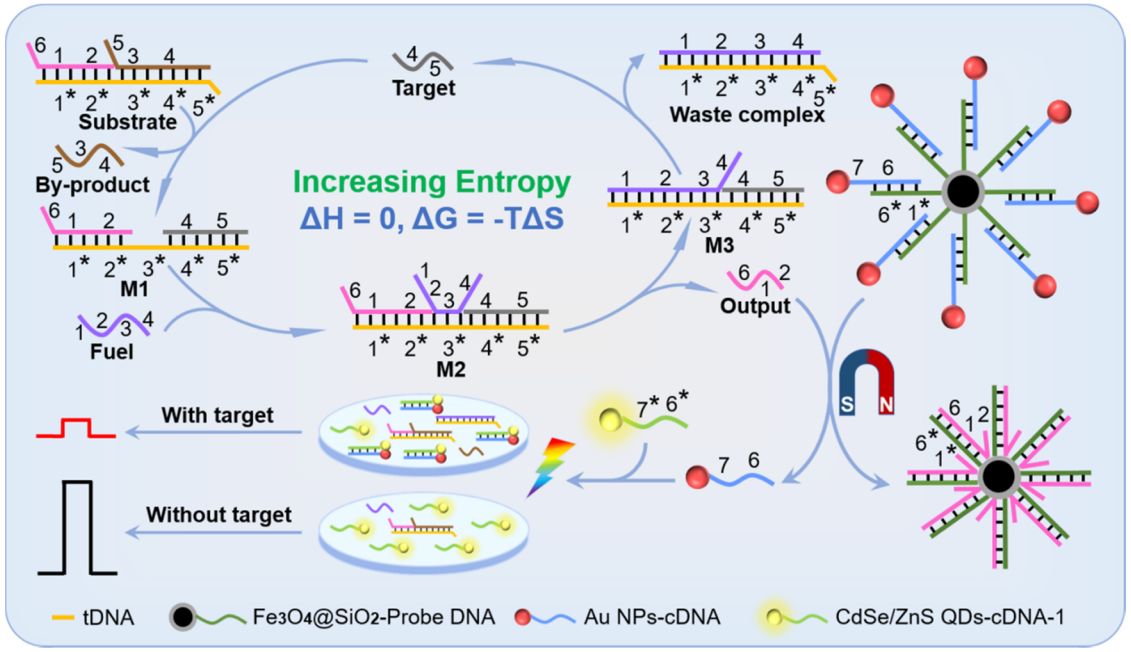

electrical signal readout endows PEC sensors with low background noise and ultrasensitivity.[26−30] For more than a decade, a variety of "signal-on" and "signal-off" PEC sensors have been developed based on photoelectric beacon strategies such as dye sensitization,[31] heterojunctions,[32,33] ion doping,[34] Z-scheme type,[35] surface plasmon resonance effect,[36] and exciton−plasmon interaction (EPI).[37] To further improve the reliability of the test results, the ratiometric[38−42] and polarity-switching-mode[43−45] PEC sensors have also been reported in recent years. In the case of EPI-based PEC sensors, the strategy is typically based on quantum dot (QD) emission and the absorption of the corresponding Au NPs, the distance between which is often regulated by changes in the structure of the DNA strand.[37,46] The design strategies all preimmobilize the biofunctionalized QDs (CdTe and Pdots) on indium tin oxide (ITO) electrodes and then introduce or release the DNA-functionalized Au NPs with the triggering of analytes. The construction of current EPI-based PEC sensors experienced multiple assembly steps and multiple washing procedures, resulting in time-consuming and unstable defects in the fabrication. Also, the unhybridized or free DNA-functionalized Au NPs may still remain on the surface of modified electrodes due to the electrostatic adsorption force. This will bring about false positive or false negative detection results. Moreover, the DNA hybridization efficiency is limited on the solid−liquid interface, which is not beneficial for the improvement of sensitivity. Therefore, eliminating the unhybridized DNA-functionalized Au NPs and generating EPI in the solution phase is beneficial for high-performance PEC biosensors.

MicroRNAs have been proved to be crucial diagnostic indicators of cancers on the basis of their abnormal expression levels. Herein, a flexible and robust EPI-based PEC biosensor was constructed with the assistance of a programmable entropy-driven DNA amplifier and the extraction of super-paramagnetic nanostructures (Scheme 1). In the absence of miRNA-let-7a as a model, the entropy-driven DNA amplifier was not triggered; with the help of magnetic separation, the only species of CdSe/ZnS QDs-cDNA-1 with an optical response remained on ITO electrodes. Then, a remarkable photocurrent was obtained with light irradiation. The presence of miRNA-let-7a can effectively initiate the entropy-driven DNA amplifier, and the released output DNAs opened the partially hybridized double-stranded DNA modified on Fe_3O_4@SiO_2 microspheres by a DNA chain replacement reaction, leading to the liberation of Au NPs-cDNA particles. With the assistance of magnetic extraction, the liberated Au NPs-cDNA completely hybridized with CdSe/ZnS QDs-cDNA-1, and the resulting EPI decreased the photocurrent of CdSe/ZnS QDs-cDNA-1. The concentration increase of miRNA-let-7a proportionally brought about the photoelectric response decrease of the as-designed PEC biosensors. Based on this working mechanism, the developed PEC biosensing platform has been used for real sample measurement. Typically, this unique one-step electrode modification avoids layer-by-layer assembly, evidently improving the electrode fabrication efficiency, reproducibility, and stability. Also, nucleic acid hybridization in the solution phase in this protocol is more in favor of the sensitivity enhancement over the conventional PEC biosensors. Moreover, the potential redundant quenching element of DNA-functionalized Au NPs anchored at the surface of Fe_3O_4@SiO_2 can be removed from the detection system, leading to the improvement of the selectivity and reliability of EPI-based PEC biosensors. The programmable entropy-driven DNA amplifier grants the as-design PEC biosensor with the advantage of ultrasensitivity as well as high selectivity. This unique design will provide a new perspective and avenue for flexible and robust PEC biosensors and also extend the application of DNA circuits.

EXPERIMENTAL SECTION

Synthesis of the Fe_3O_4@SiO_2-Probe DNA-cDNA-Au NP Complex. First, Fe_3O_4@SiO_2 particles were prepared according to the previous work,[47] and then they were dispersed in 30 mL of ethanol. After violently stirring for 5 min, 50 μL of (3-aminopropyl)triethoxysilane (APTES) were mixed and heated to reflux for 3 h. The resulting Fe_3O_4@SiO_2-NH_2

https://doi.org/10.1021/acs.analchem.1c02488
Anal. Chem. 2021, 93, 11043−11051

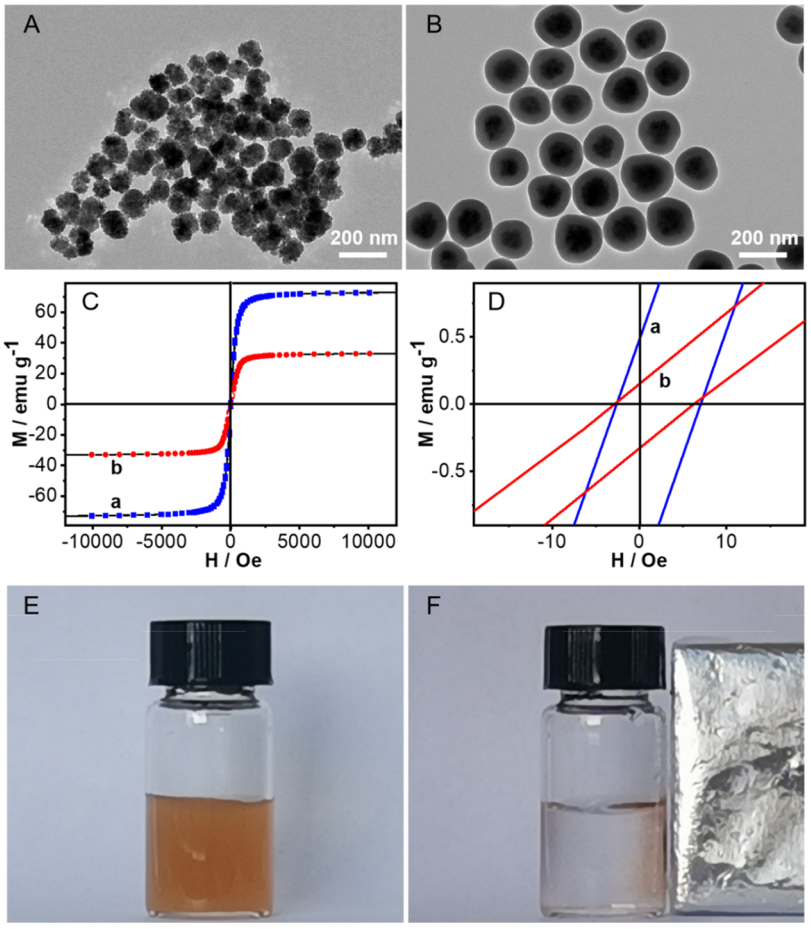

Figure 1. HRTEM images of Fe_3O_4 (A) and Fe_3O_4@SiO_2 (B). (C) The magnetic hysteresis loops of Fe_3O_4 (a) and Fe_3O_4@SiO_2 (b) and their enlarged view near the origin (D). The superparamagnetic behavior of Fe_3O_4@SiO_2 microspheres investigated at room temperature shown in (E) and (F).

microspheres were obtained by centrifugation and washed with ethyl alcohol three times, followed by dispersion in 25 mL of water. Meanwhile, probe DNA (50 μL, 10 μmol L^{-1}) was activated with 1-ethyl-3-(3-dimethylaminopropyl)carbodiimide (EDC, 25 μL, 0.1 mol L^{-1}) and *N*-hydroxysuccinimide (NHS, 25 μL, 0.025 mol L^{-1}) at 25 °C for 60 min, then they were added into 1 mL of Fe_3O_4@SiO_2-NH_2 dispersion, and the mixture reacted at 37 °C for 6 h.[48,49] With the help of magnetic separation, the Fe_3O_4@SiO_2-probe DNA was obtained and scattered into 150 μL of the buffer solution. Also, the incubation of the prepared Au NPs (0.25 mol L^{-1}, 1 mL) with capture DNA (cDNA, 10 μmol L^{-1}, 50 μL) was implemented at 37 °C overnight,[50] followed by hybridization with the prepared Fe_3O_4@SiO_2-probe DNA. After another incubation at 37 °C for 120 min,[51] the resulting Fe_3O_4@SiO_2-probe DNA-cDNA-Au NPs were collected, washed three times, and dispersed in 250 μL of the buffer solution.

Construction of the Entropy-Driven Amplifier and PEC Biosensing. For the synthesis of the substrate complex (*S*), three customized single-stranded oligonucleotides (output DNA-612, byproduct DNA-534, and template DNA-1*2*3*4*5*) were mixed in an equal molar ratio in the buffer solution.[52] The stock solution (2.0 μmol L^{-1}) was incubated at 95 °C for 5 min. When the temperature decreased to 4 °C within 1 min, it was stored in the buffer solution for future use. Subsequently, 50 μL of the buffer solution containing various concentrations of miRNA-let-7a was mixed with the substrate solution (2 μmol L^{-1}, 50 μL) and incubated at 37 °C for 120 min. The template DNA-1*2*3*4*5* (tDNA) contained a single-stranded toehold, denoted domain 5*. When miRNA-let-7a bound to domain 5*, it initiated a strand displacement reaction between domain 4 on miRNA-let-7a and the territory on byproduct DNA-534 (B). Consequently, miRNA-let-7a completely bound to tDNA and generated a metastable complex, which further released byproduct DNA-534 and formed three-stranded complex M1. After that, the fuel strand DNA-1234 (2.0 μmol L^{-1}, 50 μL) was mixed with the resulting three-stranded complex M1 and incubated at 37 °C for 120 min. Then, four-stranded complex M2 was obtained by domain 3 on fuel strand DNA-1234 (F) bound to domain 3* on M1. As a result, miRNA-let-7a was freed from metastable complex M3 with the liberation of output DNA-612 and the waste complex (W). The liberated miRNA-let-7a initiated the next round of cycle of the entropy-driven amplification procedure. After multiple cycles, the Fe_3O_4@SiO_2-probe DNA-cDNA-Au NP composite (2.0 μmol L^{-1}, 50 μL) was scattered into the mixture containing a large number of output DNA-612 and reacted for additional 120 min at 37 °C, leading to the release of cDNA-Au NPs, and the resulting Fe_3O_4@SiO_2-probe DNA-output DNA-612 and remained Fe_3O_4@SiO_2-probe DNA-cDNA-Au NP complexes were extracted by magnetic force. Meanwhile, the as-prepared CdSe/ZnS QDs (0.2 mmol L^{-1}, 100 μL) were added into 100 μL of the DNA buffer solution containing the coupling reagent

https://doi.org/10.1021/acs.analchem.1c02488
Anal. Chem. 2021, 93, 11043−11051

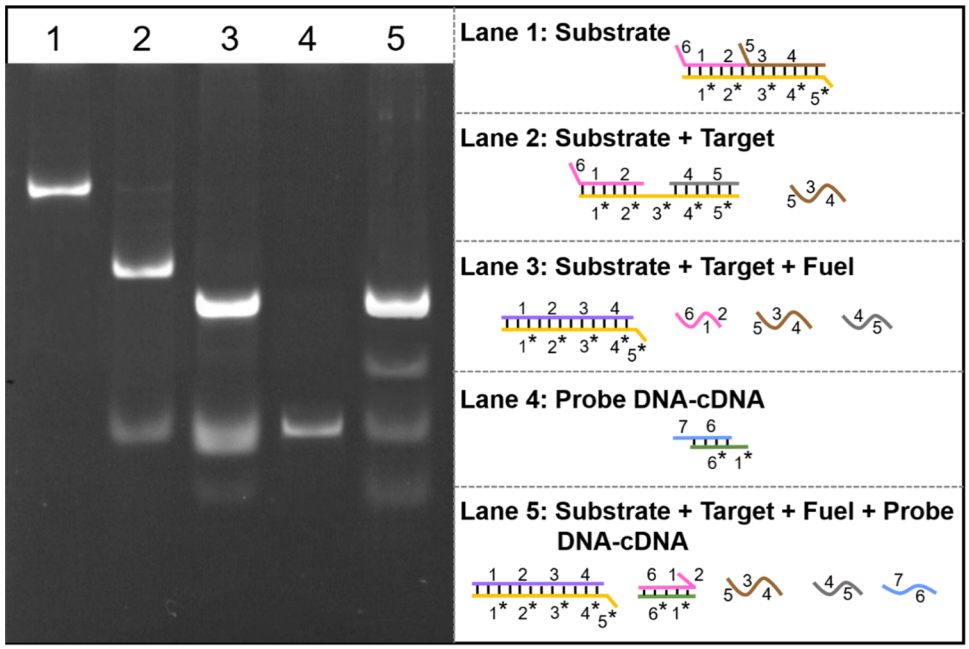

Figure 2. Electrophoretic characterization for different samples in the increasing entropy system. Lane 1: substrate: 2 μmol L^{-1} × 5 μL; lane 2: substrate: 2 μmol L^{-1} × 5 μL + target: 20 μmol L^{-1} × 0.5 μL; lane 3: substrate: 2 μmol L^{-1} × 5 μL + target: 1 μmol L^{-1} × 0.5 μL + fuel: 20 μmol L^{-1} × 0.5 μL; lane 4: probe DNA: 20 μmol L^{-1} × 0.5 μL + cDNA: 20 μmol L^{-1} × 0.5 μL; and lane 5: substrate: 2 μmol L^{-1} × 5 μL + target: 1 μmol L^{-1} × 0.5 μL + fuel: 20 μmol L^{-1} × 0.5 μL + probe DNA-cDNA: 20 μmol L^{-1} × 0.5 μL. Reaction time = 2 h.

(0.1 mol L^{-1}, 50 μL of EDC and 0.025 mol L^{-1}, 50 μL of NHS) and reacted at 25 °C for 60 min for the activation of −COOH groups on CdSe/ZnS QDs, followed by the addition of cDNA-1 (10 μmol L^{-1}, 50 μL) and reacted at 37 °C for 6 h. Afterward, 50 μL of the prepared CdSe/ZnS QDs-cDNA-1 solution was added into the entropy-driven amplification system containing the released cDNA-Au NPs and reacted for additional 120 min at 37 °C. Then, the CdSe/ZnS QDs-cDNA-1-cDNA-Au NP composite was achieved by completely Watson−Crick base pairing. Then, 20 μL of the product was modified on a cleaned ITO electrode. Subsequently, the dried photoanode was used for photocurrent acquisition in 0.1 mol L^{-1} phosphate-buffered saline (PBS, pH 7.0). In the absence of target, the entropy-driven amplifier could not be triggered, and the solution only containing CdSe/ZnS QDs-cDNA-1, substrate complex, and fuel strands was used to modify cleaned ITO electrodes with the help of magnetic extraction. Based on this entropy-driven signal amplification system, the target proportionally caused the release of output DNA-612, which resulted in the photocurrent decrease of CdSe/ZnS QDs-cDNA-1 due to the EPI in CdSe/ZnS QDs and Au NPs.

RESULTS AND DISCUSSION

Material Characterization. The morphologies and magnetic features of the synthesized functional nanomaterials were characterized using a high-resolution transmission electron microscope (HRTEM) and a superconducting quantum interference device (SQUID). As shown in Figure 1A, the average size of the synthesized Fe_3O_4 particles is approximately 91 nm. To achieve the stabilization and additional functionalization of Fe_3O_4 colloidal nanocrystalline clusters, they were coated with colloidal SiO_2, and the mean size of the resulting core−shell-structured Fe_3O_4@SiO_2 particles is ∼168 nm in diameter (Figure 1B). Figure 1C shows that the hysteresis loops measured at room temperature correspond to Fe_3O_4 and Fe_3O_4@SiO_2. Compared to the saturation magnetization of Fe_3O_4 (73.1 emu g^{-1}), it decreased to 33.1 emu g^{-1} when coated with colloidal SiO_2. Also, their hysteresis and remanence are not evidently emerged. Moreover, the coercivity in each enlarged view (Figure 1D) is not more than 20 emu g^{-1}. These indicate the superparamagnetic feature of both Fe_3O_4 and Fe_3O_4@SiO_2 particles.[53] In the presence of magnetic force, the homodispersed Fe_3O_4@SiO_2 particles can be assembled inside the flask. When the magnetic force is removed, the gathered Fe_3O_4@SiO_2 particles can also be uniformly dispersed in the aqueous phase (Figure 1E,F). This phenomenon further confirms the superparamagnetic Fe_3O_4@SiO_2. Additionally, the structures of Fe_3O_4 and Fe_3O_4@SiO_2 have been confirmed by X-ray diffraction (XRD) and X-ray photoelectron spectroscopy (XPS) in the previous work.[54]

Assessment of the Entropy-Driven Amplifier. The operation of the as-designed entropy-driven amplifier was assessed by native polyacrylamide gel electrophoresis (PAGE, Figure 2). After the reaction of equimolar amounts of output DNA-612, byproduct DNA-534, and tDNA, lane 1 shows a remarkable band, indicating the generation of the substrate complex. In contrast to the band in lane 1, the band corresponding to the substrate complex disappears and two new bands emerge in lane 2 with the introduction of equimolar miRNA-let-7a. This can be explained as follows: the toehold domain 5* in tDNA combines with miRNA-let-7a, leading to a strand displacement reaction between domain 4 on miRNA-let-7a and the territory on byproduct DNA-534 (B). As a result, miRNA-let-7a completely binds to tDNA and generates a metastable complex, which further releases byproduct DNA-534 and forms three-stranded complex M1. With the introduction of equimolar fuel strand DNA-1234 and miRNA-let-7a (0.05×) for multiple cycles, three new bands occur in lane 3, suggesting that the substrate complex is

https://doi.org/10.1021/acs.analchem.1c02488
Anal. Chem. 2021, 93, 11043−11051

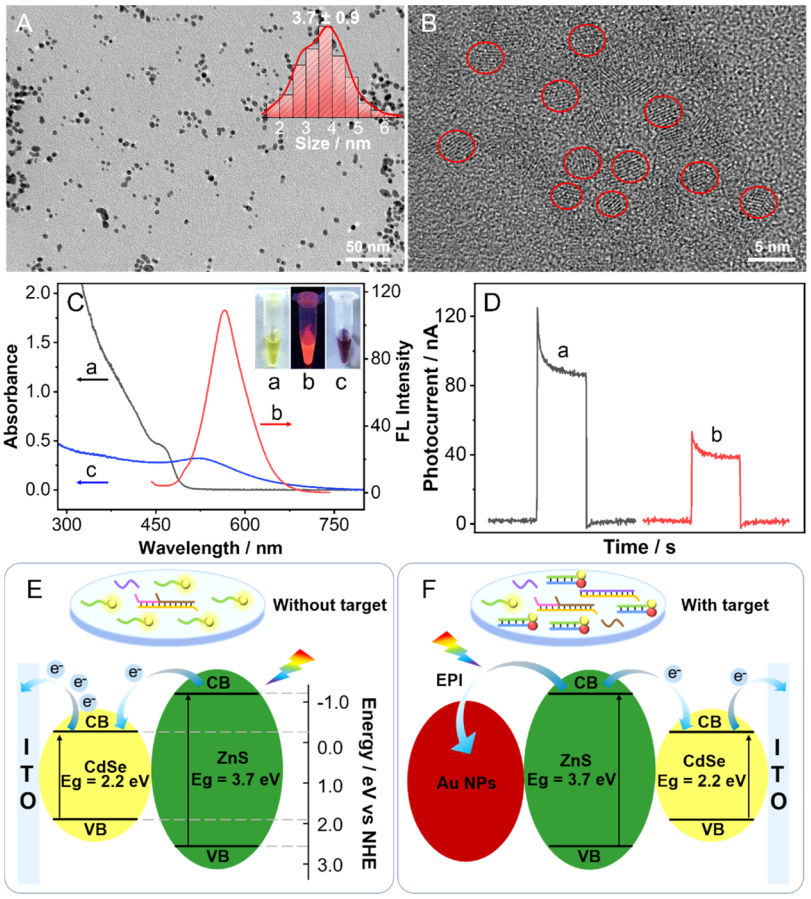

Figure 3. (A, B) HRTEM images of Au NPs and CdSe/ZnS QDs, respectively; (C) UV−vis absorption spectra of CdSe/ZnS QDs (a) and Au NPs (c) and the fluorescence emission spectrum of CdSe/ZnS QDs at a wavelength of 560 nm (b). The inset shows a digital photograph corresponding to the samples in spectra; (D) the photocurrents of CdSe/ZnS QDs (a) and the mixture containing CdSe/ZnS QDs and Au NPs-based photoanodes (b); Schematic illustrations of band energy diagram for CdSe/ZnS QDs (E) and the EPI mechanism between Au NPs and CdSe/ZnS QDs (F).

converted to the waste complex, output DNA-612, byproduct DNA-534, and miRNA-let-7a. Among them, the bands of output DNA-612 and byproduct DNA-534 cannot be distinguished due to their similar base numbers. Lane 4 shows only one band, which corresponds to the complete hybrid product of probe DNA-cDNA. When equimolar probe DNA and cDNA were introduced in the reaction system of lane 3, the appearance of a new band in lane 5 can be ascribed to the composite of probe DNA-output DNA-612 in contrast to lane 3. However, the band of cDNA cannot appear in lane 5 because its base sequence is rarely single-stranded and cannot be stained by ethidium bromide (EB). These successfully confirm that the target can efficiently trigger the operation of the entropy-driven amplifier and the released output DNA-612 can induce the DNA strand replacement reaction.

The entire entropy-driven amplification procedure marked with parameters can be represented by a reaction equation (Figure S1). The increasing entropy process is thermodynamically controlled and has been proven by the detailed calculation in the Supporting Information.

Photoelectric Response Working Mechanism. Figure 3A,B exhibits the HRTEM images of Au NPs and CdSe/ZnS QDs, respectively. Figure 3C shows UV−vis spectra, fluorescence spectra, and the corresponding digital photographs of CdSe/ZnS QDs and Au NPs. As is shown, the emission spectrum of CdSe/ZnS QDs overlaps well with the absorption spectrum of Au NPs, resulting in the EPI between them.[37] As shown in Figure 3D, the CdSe/ZnS QD-based photoanode exhibits a remarkable photocurrent of 124.5 nA. However, when the Au NPs were introduced in the CdSe/ZnS QD-based photoanode, the photocurrent obviously decreases to 50.2 nA, which is resulted from the EPI in CdSe/ZnS QDs and Au NPs.[37] The detailed PEC working mechanism is proposed in Figure 3E,F. Without the initiation of miRNA-let-7a, the entropy-driven DNA amplifier cannot operate. With the assistance of magnetic separation, the only species of CdSe/ZnS QDs-cDNA-1 with an optical response remained on ITO electrodes. Under light irradiation, given the energy level matching between them, the photoelectrons resulted from ZnS QDs transfer to the conduction band (CB) of CdSe QDs and then transfer to the external circuit, bringing about a remarkable photoelectric response. However, the target can initiate the entropy-driven amplifier, and the released output DNAs open the partially hybridized double-stranded DNA modified on Fe_3O_4@SiO_2 microspheres by the DNA chain replacement reaction, leading to the liberation of Au NPs-cDNA particles. With magnetic assistance, the liberated Au NPs-cDNA completely hybridized with CdSe/ZnS QDs-cDNA-1 by Watson−Crick base pairing and resulted in the weakened photocurrent (Figure 3F). Based on this PEC principle, a unique and flexible EPI-based PEC biosensor for miRNA-let-7a can be developed with the assistance of the

https://doi.org/10.1021/acs.analchem.1c02488
Anal. Chem. 2021, 93, 11043−11051

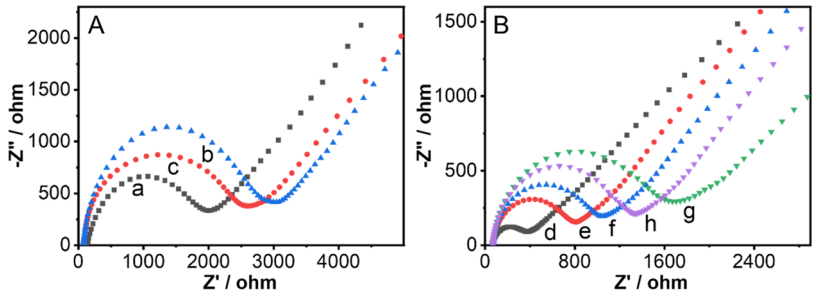

Figure 4. Electrochemical impedance spectra of (a) Fe_3O_4@SiO_2-NH_2, (b) Fe_3O_4@SiO_2-probe DNA, (c) Fe_3O_4@SiO_2-probe DNA-cDNA-Au NPs, (d) Au NPs, (e) Au NPs-cDNA, (f) CdSe/ZnS QDs, (g) CdSe/ZnS QDs-cDNA-1, and (h) Au NPs- cDNA-cDNA-1-CdSe/ZnS QD-modified glassy carbon electrodes in a 2.5 mmol L^{-1} $K_4Fe(CN)_6$ and $K_3Fe(CN)_6$ solution containing 0.2 mol L^{-1} KCl.

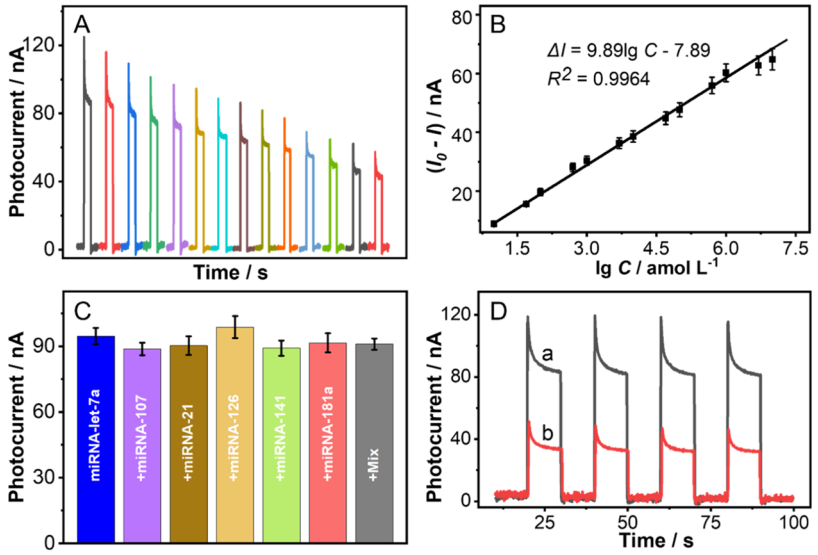

Figure 5. (A) Photocurrent corresponding to the concentration of 0, 10, 50, 100, 500 amol L^{-1}, 1, 5, 10, 50, 100, 500 fmol L^{-1}, 1, 5, and 10 pmol L^{-1} miRNA-let-7a in 0.1 mol L^{-1} PBS (pH 7.0). (B) The linear calibration curve. (C) Interference investigated by conventional miRNAs with different concentrations. (D) Photocurrent responses of the PEC biosensor in the presence of 10 amol L^{-1} and 10 pmol L^{-1} miRNA-let-7a in 0.1 mol L^{-1} PBS (pH 7.0) with chopped light irradiation.

Table 1. Comparison of the Different Detection Methods for miRNA-let-7a

analytical method	detection limit	linear range	references
colorimetric	21.7 pmol L^{-1}	50 pmol L^{-1} to 10 nmol L^{-1}	55
fluorescence	67.3 fmol L^{-1}	100 fmol L^{-1} to 50 pmol L^{-1}	56
fluorescence	10.8 fmol L^{-1}	60 fmol L^{-1} to 12 pmol L^{-1}	57
chemiluminescence resonance energy transfer imaging	6.9 fmol L^{-1}	10 fmol L^{-1} to 100 pmol L^{-1}	58
fluorescence	4.6 fmol L^{-1}	5 fmol L^{-1} to 5 pmol L^{-1}	59
electrochemiluminescence	1.49 fmol L^{-1}	10 fmol L^{-1} to 10 nmol L^{-1}	60
electrochemical	25 amol L^{-1}	80 amol L^{-1} to 300 fmol L^{-1}	61
electrochemical	0.25 nmol L^{-1}	0.4−140 nmol L^{-1}	63
fluorescence	35 amol L^{-1}	0.1 fmol L^{-1} to 10 pmol L^{-1}	64
photoelectrochemical	3.35 amol L^{-1}	10 amol L^{-1} to 1 pmol L^{-1}	this work

programmable entropy-driven DNA amplifier and superparamagnetic nanostructures.

Electrode Modification Assessment. Electrochemical impedance spectroscopy (EIS) was chosen to assess the assembled Fe_3O_4@SiO_2-probe DNA-cDNA-Au NPs and Au NPs-cDNA-cDNA-1-CdSe/ZnS QDs. As shown in Figure 4A, compared to a charge-transfer resistance (R_{ct}) value of 2001 Ω from the semicircle Nyquist plots (curve a), the R_{ct} value of curve b increased to 2997 Ω, ascribing to the nonconductive probe DNA anchored on Fe_3O_4@SiO_2 particles. However, the R_{ct} of curve c decreases to 2560 Ω, which can be attributed to Au NPs with excellent electrical conductivity since cDNA-Au NPs successfully hybridized to probe DNA, resulting in the generation of the Fe_3O_4@SiO_2-probe DNA-cDNA-Au NP composite. A similar mechanism can be utilized for the expression of the successfully prepared Au NPs-cDNA, CdSe/ZnS QDs-cDNA-1, and Au NPs-cDNA-cDNA-1-CdSe/ZnS QD composites (Figure 4B).

Analytical Performance. The developed PEC biosensing platform was applied to detecting miRNA-let-7a with the assistance of the programmable entropy-driven DNA amplifier and the extraction of superparamagnetic nanostructures

https://doi.org/10.1021/acs.analchem.1c02488
Anal. Chem. 2021, 93, 11043−11051

(Figure 5). As shown in Figure 5A, with the increase in the concentration of miRNA-let-7a, the photocurrent gradually decreased (Figure 5A). A praiseworthy linear relationship between the change of PEC signal intensity and the logarithm of miRNA-let-7a concentration was established. Herein, I_0 and I represent the photocurrent intensity in the absence and presence of target, respectively. The dynamic linear range between 10 amol L^{-1} and 1 pmol L^{-1} was evaluated by photocurrent decrease versus lg *C*. The linear regression equation was $\Delta I = 9.89 \lg C - 7.89$ (Figure 5B) with a detection limit of 3.35 amol L^{-1} at 3 S/N, which is advantageous over the reported colorimetric (21.7 pmol L^{-1}),[55] fluorescence (67.3, 10.8, 4.6 fmol L^{-1}, 35 amol L^{-1}),[56,57,59,64] chemiluminescence resonance energy transfer imaging (6.9 fmol L^{-1}),[58] electrochemiluminescence (1.49 fmol L^{-1}),[60] and electrochemistry (25 amol L^{-1}, 0.25 nmol L^{-1})[61,63] approaches. This ultrasensitive detection method mainly derives from the entropy-driven signal amplification, DNA hybridization in the solution phase, and the ultrasensitive nature inherent in PEC sensing.[62] Moreover, the PEC biosensor with 5 orders of magnitude is comparable to almost all of the reported ones shown in Table 1. Compared to the reported EPI-based PEC sensing design,[37,46] the as-designed PEC biosensor holds an additional advantage of electrode fabrication efficiency, which benefits from the single-step electrode modification procedure instead of the conventional layer-by-layer assembly.

Selectivity as an important parameter was evaluated by the potential interference species including miRNA-107, miRNA-21, miRNA-126, miRNA-141, and miRNA-181a. As shown in Figure 5C, each added coexistence species with 500 times the concentration of miRNA-let-7a (1 fmol L^{-1}) and a mixture of the above miRNAs (each 100 times) almost do not change the photocurrent in contrast to that of miRNA-let-7a itself. The maximum photocurrent change does not exceed 10%, suggesting the fabricated PEC biosensor with remarkable selectivity. It can be attributed to the Watson−Crick base pairing rule and the entropy-driven DNA amplifier. Additionally, the potential redundant quenching element of DNA-functionalized Au NPs anchored at the surface of Fe_3O_4@SiO_2 can be removed from the detection system, leading to the improvement of the selectivity and reliability of the as-designed PEC biosensors.

Stability as a crucial factor was also inspected by the chopped photoelectric response. As shown in Figure 5D, the photocurrents are almost unchanged for 10 amol L^{-1} and 10 pmol L^{-1} miRNA-let-7a with consecutive four cycles of chopped light illumination, suggesting the favorable short-term stability. Also, the long-term stability of the PEC biosensor has been appraised by the photocurrent measurement every week (Figure S2). The photocurrent almost remains the same after four weeks, indicating that the PEC sensor has satisfied stability. Moreover, the repeatability has been evaluated by six freshly fabricated PEC biosensors. A relative standard deviation (RSD) of 5.1% calculated from the working curves (Figure 5B) indicates excellent manufacturing reproducibility. These can be attributed to the single-step electrode modification procedure rather than the layer-by-layer assembly and subsequent multistep washing.

The utility of the proposed protocol in real samples was also investigated by the standard addition method. As shown in Table 2, the recovery is between 94.6 and 106.5%, and the RSD is less than 4.36%. These suggest the acceptable accuracy of the as-designed PEC biosensors for real sample measurement.

Table 2. Developed PEC Biosensor Utilized for the Measurement of miRNA-let-7a in Serum Samples (n = 4)[a]

sample	added (amol L^{-1})	found (amol L^{-1})	recovery (%)	RSD (%)
human serum	0			
	10	9.46	94.6	4.36
	100	106.53	106.5	3.49
	1000	957.93	95.8	2.57

[a] n is the repetitive measurement number.

CONCLUSIONS

In summary, programmable DNA nanotechnology has been successfully applied in the construction of a flexible and elegant PEC platform for low-abundance miRNA-let-7a in real serum samples. This unique entropy-driven amplification strategy helps reduce the reversibility of each step of the reaction, keeps the base sequence intact, improves reaction efficiency, and exhibits high thermal stability, specificity, and flexible design. The as-designed high-performance PEC biosensor can be attributed to the extraordinary entropy-driven DNA amplification strategy, superparamagnetic Fe_3O_4@SiO_2 particles, DNA hybridization in the solution phase rather than on solid−liquid interface assembly, and single-step electrode modification procedure. These enable the as-designed PEC biosensor to possess advantages of ultrasensitivity and high specificity, as well as high electrode fabrication efficiency, reproducibility, and stability. The operation of the entropy-driven amplifier was validated by PAGE description and calculated using thermodynamics. Moreover, the EPI-based photoelectric response working mechanism was proposed by UV−vis, fluorescence spectra, and their corresponding photocurrent response. This unique design expands the application of DNA circuits and provides a new perspective for remarkably improving the detection performance of various low-abundance miRNAs. It is promising for future clinical applications based on this flexible and robust PEC biosensor.

ASSOCIATED CONTENT

Supporting Information

The Supporting Information is available free of charge at https://pubs.acs.org/doi/10.1021/acs.analchem.1c02488.

Reagents and apparatus; synthesis of Fe_3O_4 colloidal nanocrystal clusters, Fe_3O_4@SiO_2 particles, Au nanoparticles, and CdSe/ZnS quantum dots; native gel electrophoresis characterization; thermodynamic calculation of the entropy-driven system; and another test (Figure S2) (PDF)

AUTHOR INFORMATION

Corresponding Authors

Hongbo Li − *School of Chemistry and Chemical Engineering, Yancheng Institute of Technology, Yancheng 224051, P. R. China*; orcid.org/0000-0001-8662-0427; Phone: +86-515-88298735; Email: hbli@ycit.edu.cn

Jing Li − *School of Chemistry and Chemical Engineering, Yancheng Institute of Technology, Yancheng 224051, P. R. China*; Email: jli@ycit.edu.cn

https://doi.org/10.1021/acs.analchem.1c02488
Anal. Chem. 2021, 93, 11043−11051

Authors

Ye Cao − *School of Chemistry and Chemical Engineering, Yancheng Institute of Technology, Yancheng 224051, P. R. China*

Tianyu Wu − *School of Chemistry and Chemical Engineering, Yancheng Institute of Technology, Yancheng 224051, P. R. China*

Yansong Zhang − *School of Chemistry and Chemical Engineering, Yancheng Institute of Technology, Yancheng 224051, P. R. China*

Zhaoting Zheng − *School of Chemistry and Chemical Engineering, Yancheng Institute of Technology, Yancheng 224051, P. R. China*

Jingchun Lv − *School of Chemistry and Chemical Engineering, Yancheng Institute of Technology, Yancheng 224051, P. R. China*

Airong Mao − *School of Chemistry and Chemical Engineering, Yancheng Institute of Technology, Yancheng 224051, P. R. China*

Yuye Zhang − *School of Chemistry and Chemical Engineering, Yancheng Institute of Technology, Yancheng 224051, P. R. China*

Qin Tang − *School of Chemistry and Chemical Engineering, Yancheng Institute of Technology, Yancheng 224051, P. R. China*

Complete contact information is available at: https://pubs.acs.org/10.1021/acs.analchem.1c02488

Notes

The authors declare no competing financial interest.

■ ACKNOWLEDGMENTS

The authors acknowledge the financial support from the Natural Science Foundation of China (21505117 and 21775135) and the Natural Science Foundation of Jiangsu Province (BK20161309 and BK20201473), and this work was also sponsored by Qinglan Project of Jiangsu Province.

■ REFERENCES

(1) Dong, Y.; Yao, C.; Zhu, Y.; Yang, L.; Luo, D.; Yang, D. *Chem. Rev.* **2020**, *120*, 9420−9481.
(2) Seeman, N. C.; Sleiman, H. F. *Nat. Rev. Mater.* **2018**, *3*, No. 17068.
(3) Nummelin, S.; Kommeri, J.; Kostiainen, M. A.; Linko, V. *Adv. Mater.* **2018**, *30*, No. 1703721.
(4) Mergny, J. L.; Sen, D. *Chem. Rev.* **2019**, *119*, 6290−6325.
(5) Fan, C. H.; Li, Q. *Small* **2019**, *15*, No. 1902586.
(6) Seeman, N. C. *J. Theor. Biol.* **1982**, *99*, 237−247.
(7) Rizzuto, F. J.; Trinh, T.; Sleiman, H. F. *Chem* **2020**, *6*, 1560−1574.
(8) Platnich, C. M.; Rizzuto, F. J.; Cosa, G.; Sleiman, H. F. *Chem. Soc. Rev.* **2020**, *49*, 4220−4233.
(9) Turberfield, A. J. *Nat. Chem.* **2011**, *3*, 580−581.
(10) Zhang, F.; Yan, H. *Nature* **2017**, *552*, 34−35.
(11) Chen, Y. J.; Groves, B.; Muscat, R. A.; Seelig, G. *Nat. Nanotechnol.* **2015**, *10*, 748−760.
(12) Zhang, D. Y.; Seelig, G. *Nat. Chem.* **2011**, *3*, 103−113.
(13) Wang, S. S.; Ellington, A. D. *Chem. Rev.* **2019**, *119*, 6370−6383.
(14) Arter, W. E.; Yusim, Y.; Peter, Q.; Taylor, C. G.; Klenerman, D.; Keyser, U. F.; Knowles, T. P. J. *ACS Nano* **2020**, *14*, 5763−5771.
(15) Guo, Y.; Yao, D.; Zheng, B.; Sun, X.; Zhou, X.; Wei, B.; Xiao, S.; He, M.; Li, C.; Liang, H. *ACS Nano* **2020**, *14*, 8317−8327.
(16) Li, H.; Han, M.; Weng, X.; Zhang, Y.; Li, J. *ACS Nano* **2021**, *15*, 1710−1717.
(17) Li, J.; Weng, X.; Mo, F.; Han, M.; Li, H. *Anal. Chem.* **2020**, *92*, 15145−15151.
(18) Lv, Y.; Cui, L.; Peng, R.; Zhao, Z.; Qiu, L.; Chen, H.; Jin, C.; Zhang, X. B.; Tan, W. *Anal. Chem.* **2015**, *87*, 11714−11720.
(19) Liang, C. P.; Ma, P. Q.; Liu, H.; Guo, X.; Yin, B. C.; Ye, B. C. *Angew. Chem., Int. Ed.* **2017**, *56*, 9077−9081.
(20) He, L.; Lu, D.; Liang, H.; Xie, S.; Zhang, X.; Liu, Q.; Yuan, Q.; Tan, W. *J. Am. Chem. Soc.* **2018**, *140*, 258−263.
(21) Li, C.; Wang, H.; Shang, J.; Liu, X.; Yuan, B.; Wang, F. *ACS Sens.* **2018**, *3*, 2359−2366.
(22) Ma, F.; Wei, S. H.; Zhang, C. Y. *Anal. Chem.* **2019**, *91*, 7505−7509.
(23) Simmel, F. C.; Yurke, B.; Singh, H. R. *Chem. Rev.* **2019**, *119*, 6326−6369.
(24) Meng, H. M.; Shi, X.; Chen, J.; Gao, Y.; Qu, L.; Zhang, K.; Zhang, X. B.; Li, Z. *ACS Sens.* **2020**, *5*, 103−109.
(25) Peng, H.; Newbigging, A. M.; Reid, M. S.; Uppal, J. S.; Xu, J.; Zhang, H.; Le, X. C. *Anal. Chem.* **2020**, *92*, 292−308.
(26) Shu, J.; Tang, D. *Anal. Chem.* **2020**, *92*, 363−377.
(27) Hou, T.; Xu, N.; Wang, W.; Ge, L.; Li, F. *Anal. Chem.* **2018**, *90*, 9591−9597.
(28) Wang, Z.; Liu, J.; Liu, X.; Shi, X.; Dai, Z. *Anal. Chem.* **2019**, *91*, 830−835.
(29) Zhang, G. Y.; Zhuang, Y. H.; Shan, D.; Su, G. F.; Cosnier, S.; Zhang, X. J. *Anal. Chem.* **2016**, *88*, 11207−11212.
(30) Ma, W.; Ma, H.; Peng, Y. Y.; Tian, H.; Long, Y. T. *Nat. Protoc.* **2019**, *14*, 2672−2690.
(31) Li, M.; Xiong, C.; Zheng, Y.; Liang, W.; Yuan, R.; Chai, Y. *Anal. Chem.* **2018**, *90*, 8211−8216.
(32) Peng, J.; Huang, Q.; Zhuge, W.; Liu, Y.; Zhang, C.; Yang, W.; Xiang, G. *Biosens. Bioelectron.* **2018**, *106*, 212−218.
(33) Peng, J.; Huang, Q.; Liu, Y.; Liu, P.; Zhang, C. *Sens. Actuators, B* **2019**, *294*, 157−165.
(34) Li, H.; Li, J.; Zhu, Y.; Xie, W.; Shao, R.; Yao, X.; Gao, A.; Yin, Y. *Anal. Chem.* **2018**, *90*, 5496−5502.
(35) Zhu, J. H.; Feng, Y. G.; Wang, A. J.; Mei, L. P.; Luo, X.; Feng, J. J. *Biosens. Bioelectron.* **2021**, *181*, No. 113158.
(36) Zhao, C. Q.; Zhou, J.; Wu, K. W.; Ding, S. N.; Xu, J. J.; Chen, H. Y. *Anal. Chem.* **2020**, *92*, 6886−6892.
(37) Zeng, X.; Ma, S.; Bao, J.; Tu, W.; Dai, Z. *Anal. Chem.* **2013**, *85*, 11720−11724.
(38) Yang, H.; Hu, M.; Li, Z.; Zhao, P.; Xie, L.; Song, X.; Yu, J. *Anal. Chem.* **2019**, *91*, 14577−14585.
(39) Fu, B.; Zhang, Z. *Anal. Chem.* **2019**, *91*, 14829−14833.
(40) Hao, N.; Hua, R.; Zhang, K.; Lu, J.; Wang, K. *Anal. Chem.* **2018**, *90*, 13207−13211.
(41) Zheng, Y. N.; Liang, W. B.; Xiong, C. Y.; Zhuo, Y.; Chai, Y. Q.; Yuan, R. *Anal. Chem.* **2017**, *89*, 9445−9451.
(42) Hao, Q.; Shan, X.; Lei, J.; Zang, Y.; Yang, Q.; Ju, H. *Chem. Sci.* **2016**, *7*, 774−780.
(43) Fu, Y.; Xiao, K.; Zhang, X.; Du, C.; Chen, J. *Anal. Chem.* **2021**, *93*, 1076−1083.
(44) Fu, Y.; Zou, K.; Liu, M.; Zhang, X.; Du, C.; Chen, J. *Anal. Chem.* **2020**, *92*, 1189−1196.
(45) Mo, F.; Han, M.; Weng, X.; Zhang, Y.; Li, J.; Li, H. *Anal. Chem.* **2020**, *93*, 1764−1770.
(46) Zhang, N.; Shi, X. M.; Guo, H. Q.; Zhao, X. Z.; Zhao, W. W.; Xu, J. J.; Chen, H. Y. *Anal. Chem.* **2018**, *90*, 11892−11898.
(47) Li, H.; Li, Y.; Li, J.; Yang, F.; Xu, L.; Wang, W.; Yao, X.; Yin, Y. *Anal. Chem.* **2020**, *92*, 4094−4100.
(48) Gao, X.; Cai, Q.; Li, H.; Jie, G. *Anal. Chem.* **2020**, *92*, 6734−6740.
(49) Jie, G.; Li, C.; Zhao, Y.; Kuang, Q.; Niu, S. *ACS Appl. Nano Mater.* **2019**, *2*, 4637−4645.
(50) Sun, Y.; Shi, L.; Wang, Q.; Mi, L.; Li, T. *Anal. Chem.* **2019**, *91*, 3652−3658.
(51) Xu, Z. H.; Wang, H.; Wang, J.; Zhao, W.; Xu, J. J.; Chen, H. Y. *Anal. Chem.* **2019**, *91*, 12000−12005.

(52) Wang, S.; Song, W.; Wei, S.; Zeng, S.; Yang, S.; Lei, C.; Huang, Y.; Nie, Z.; Yao, S. *Anal. Chem.* **2019**, *91*, 8622−8629.
(53) Peng, S.; Lei, C.; Ren, Y.; Cook, R. E.; Sun, Y. *Angew. Chem., Int. Ed.* **2011**, *50*, 3158−3163.
(54) Li, J.; Xu, L.; Shen, Y.; Guo, L.; Yin, H.; Fang, X.; Yang, Z.; Xu, Q.; Li, H. *Anal. Chem.* **2020**, *92*, 8607−8613.
(55) Chen, W.; Zhang, X.; Li, J.; Chen, L.; Wang, N.; Yu, S.; Li, G.; Xiong, L.; Ju, H. *Anal. Chem.* **2020**, *92*, 2714−2721.
(56) Tang, X.; Deng, R.; Sun, Y.; Ren, X.; Zhou, M.; Li, J. *Anal. Chem.* **2018**, *90*, 10001−10008.
(57) Liu, H.; Li, L.; Wang, Q.; Duan, L.; Tang, B. *Anal. Chem.* **2014**, *86*, 5487−5493.
(58) Bi, S.; Xiu, B.; Ye, J.; Dong, Y. *ACS Appl. Mater. Interfaces* **2015**, *7*, 23310−23319.
(59) Ge, J.; Hu, Y.; Deng, R.; Li, Z.; Zhang, K.; Shi, M.; Yang, D.; Cai, R.; Tan, W. *Anal. Chem.* **2020**, *92*, 13588−13594.
(60) Zhao, M. L.; Zeng, W. J.; Chai, Y. Q.; Yuan, R.; Zhuo, Y. *Anal. Chem.* **2020**, *92*, 11044−11052.
(61) Ge, L.; Wang, W.; Li, F. *Anal. Chem.* **2017**, *89*, 11560−11567.
(62) Song, X.; Hou, T.; Lu, F.; Wang, Y.; Liu, J.; Li, F. *Chem. Commun.* **2020**, *56*, 1811−1814.
(63) Wu, J.; Lv, W.; Yang, Q.; Li, H.; Li, F. *Biosens. Bioelectron.* **2021**, *171*, No. 112707.
(64) Li, H.; Chang, J.; Gai, P.; Li, F. *ACS Appl. Mater. Interfaces* **2018**, *10*, 4561−4568.

https://doi.org/10.1021/acs.analchem.1c02488
Anal. Chem. 2021, 93, 11043−11051